PAPER • OPEN ACCESS

Generating *T* centres in photonic silicon-on-insulator material by ion implantation

New Journal of Physics
The open access journal at the forefront of physics

Deutsche Physikalische Gesellschaft DPG
IOP Institute of Physics

Published in partnership with: Deutsche Physikalische Gesellschaft and the Institute of Physics

OPEN ACCESS

RECEIVED
24 March 2021

REVISED
19 August 2021

ACCEPTED FOR PUBLICATION
22 September 2021

PUBLISHED
8 October 2021

PAPER

Generating *T* centres in photonic silicon-on-insulator material by ion implantation

E R MacQuarrie[1,2], C Chartrand[1], D B Higginbottom[1], K J Morse[1,2], V A Karasyuk[1], S Roorda[3] and S Simmons[1,2,*]

[1] Department of Physics, Simon Fraser University, Burnaby, British Columbia, Canada
[2] Photonic Inc., Vancouver, British Columbia, Canada
[3] Department of Physics, Université de Montréal, Montreal, Quebec, Canada
[*] Author to whom any correspondence should be addressed.

E-mail: s.simmons@sfu.ca

Keywords: colour centres, spin-photon interfaces, silicon photonics, silicon spin qubits

Supplementary material for this article is available online

Abstract

Global quantum networks will benefit from the reliable fabrication and control of high-performance solid-state telecom photon-spin interfaces. *T* radiation damage centres in silicon provide a promising photon-spin interface due to their narrow *O*-band optical transition near 1326 nm and long-lived electron and nuclear spin lifetimes. To date, these defect centres have only been studied as ensembles in bulk silicon. Here, we fabricate high concentration *T* centre ensembles in the 220 nm device layer of silicon-on-insulator wafers by ion implantation and subsequent annealing. We then develop a method that uses spin-dependent optical transitions to benchmark the characteristic optical spectral diffusion within these *T* centre ensembles. Using this new technique, we show that with minimal optimization to the fabrication process high densities of implanted *T* centres localized $\lesssim$100 nm from an interface display $\sim$1 GHz characteristic levels of total spectral diffusion.

1. Introduction

Point defect colour centres in solid state systems provide a promising platform for emerging quantum technologies. A number of colour centres are currently in development [1, 2], but few of these leading candidates are both natively integrated into silicon and intrinsically operate at telecom wavelengths. Radiation damage centres in silicon have recently emerged as promising light–matter interfaces that simultaneously meet both of these criteria [3–6]. Within this family of defects, the *T* centre notably possesses highly coherent electron and nuclear spin degrees of freedom and narrow, spin-dependent ensemble optical transitions near 1326 nm in the telecommunications *O*-band [7]. These properties make the *T* centre a competitive candidate for integration into future commercial-scale quantum networks with long-lived quantum memory and computing capabilities.

Incorporating *T* centres into such quantum networks requires a reliable means of making the centres in device-ready material such as silicon-on-insulator (SOI). Ion implantation and thermal treatment have previously been used to generate spin-photon interfaces in non-silicon host materials [8–11] and colour centres in silicon that lack a demonstrated spin degree of freedom [5, 6, 12, 13]. Here, we provide the first demonstration of generating *T* centres in SOI by ion implantation and subsequent annealing. In the 220 nm device layer of commercial SOI wafers, we achieve high *T* centre concentrations that are $>$30 times higher than in previously measured bulk samples and, in follow-on work [14], present evidence that these SOI concentrations are $>1.7 \times 10^{13}$ cm^{-3}. Moreover, in comparable bulk material, the inhomogeneous broadening of the zero phonon line (ZPL) within implanted ensembles can be only $\sim$35% larger than in *T* centre ensembles generated by electron irradiation and annealing, suggesting that the additional lattice

damage generated by ion implantation does not dramatically broaden the distribution of local environments within our samples.

The fabrication process used to generate T centres should preserve the excellent spin and optical properties that T centre ensembles exhibit in bulk silicon where the majority of centres are located far from material interfaces. The increase in electric and magnetic field noise near those interfaces can dramatically degrade a centre's spin and optical properties. Encouragingly, donor spin defects in silicon have already demonstrated competitive coherence times for electron (0.95 ms Hahn echo T_2) and nuclear (20 ms Hahn echo T_2 in the neutral donor state) spins at distances of just 10 nm from $^{28}Si/SiO_2$ interfaces [15]. T centres at our target depth of 110 nm could demonstrate comparably high-quality spin coherence.

In the optical domain, spectral diffusion—the time-varying changes in a centre's optical transition energies—often dominates the optical properties of emitters located near interfaces. Spectral diffusion can reduce the indistinguishability of emitted photons, limiting an emitter's potential in quantum technologies. Measuring the characteristic spectral diffusion of the generated T centre ensembles thus provides an important metric for benchmarking our fabrication process. To this end, we develop a method that uses spin-dependent optical transitions to efficiently measure the characteristic long-term (total) spectral diffusion within an ensemble of emitters.

Applying this new technique to our high-concentration T centre ensembles in SOI, we measure characteristic total spectral diffusion of $\sim$1 GHz. Although this value is $\sim 10^4$ times larger than the 169 kHz lifetime-limited linewidth, excellent photon indistinguishability could still be achieved by employing fabrication or measurement techniques designed to stabilize the electromagnetic environment [16–19], by filtering the emitted photons [20, 21], or by Purcell-enhancing the radiative decay rate [22, 23] as the T centre is expected to have a high radiative efficiency [7]. Critically, by hosting T centres within the SOI device layer itself, it becomes possible to design fully-integrated quantum networks where a T centre's spin-dependent emission never has to leave the Si device layer from generation, through processing, to detection. Such an approach would mitigate the challenge of extracting single photons from high-index host materials.

2. T centre implantation

As shown in figure 1(a), the T centre is thought to consist of two carbon atoms sharing the substitutional site of one silicon atom; an interstitial hydrogen terminates one of these carbon atoms while the other remains stable with an unpaired electron [24]. The current formation model for this defect consists of an interstitial carbon capturing a hydrogen atom and then migrating to a substitutional carbon site during heat treatment at temperatures between 350°C and 600°C [7, 24]. Starting from SOI with a 220 nm thick Czochralski (CZ) natural Si (^{nat}Si) device layer and 3 μm of buried SiO_2, we realize this formation process by implanting carbon and then hydrogen in a fixed [C:H] = 1:1 fluence ratio, annealing between the two implants and then annealing again after the hydrogen implant.

We performed two fabrication runs: one with a ^{12}C implant and fluences of 7×10^{12} cm^{-2} and a second with ^{13}C and fluences of 7×10^{13} cm^{-2}. These fluences, which were chosen from measurements detailed in the supplementary materials (SM) (https://stacks.iop.org/NJP/23/103008/mmedia) [25], place the initial carbon concentrations well above the carbon solubility limit for silicon at 1000°C [26]. Carbon implants were performed at an energy of 38 keV, while hydrogen was implanted at 9 keV to target overlapping implantation profiles with a mean depth of 110 nm.

In between the two implants, we performed a rapid thermal anneal at 1000°C for 20 s in an argon background to repair lattice damage generated during the carbon implant and to incorporate carbon onto substitutional lattice sites [5, 27]. The subsequent hydrogen implant then generates lattice damage and interstitial carbon to promote T centre formation, but the smaller mass of the hydrogen ions generates less total damage than the carbon implant [25]. After the hydrogen implant, we boiled the samples for 1 h in deionized water to further increase the hydrogen concentration [25, 28] before performing a final rapid thermal anneal for 3 min at a temperature ranging from 345°C to 480°C in a nitrogen atmosphere.

Figure 1(b) shows the integrated area of the T centre ZPL as a function of the final anneal temperature for a series of SOI samples. For these samples, we find optimum temperatures of 400°C for a fluence of 7×10^{12} cm^{-2} and 420°C for 7×10^{13} cm^{-2}. Unless otherwise noted, we have normalized photoluminescence (PL) spectra to the free exciton (FE) recombination line at $\sim$ 1097 meV. Although the FE recombination line can vary in intensity across samples as, for instance, the density of recombination sites changes, it provides a means of roughly quantifying the T centre concentration to enable comparison amongst samples [25, 29].

In figures 1(c) and (d), we plot the PL spectra under above-band (532 nm) excitation for these particular SOI samples alongside that of an isotopically-purified ^{28}Si bulk sample with a carbon

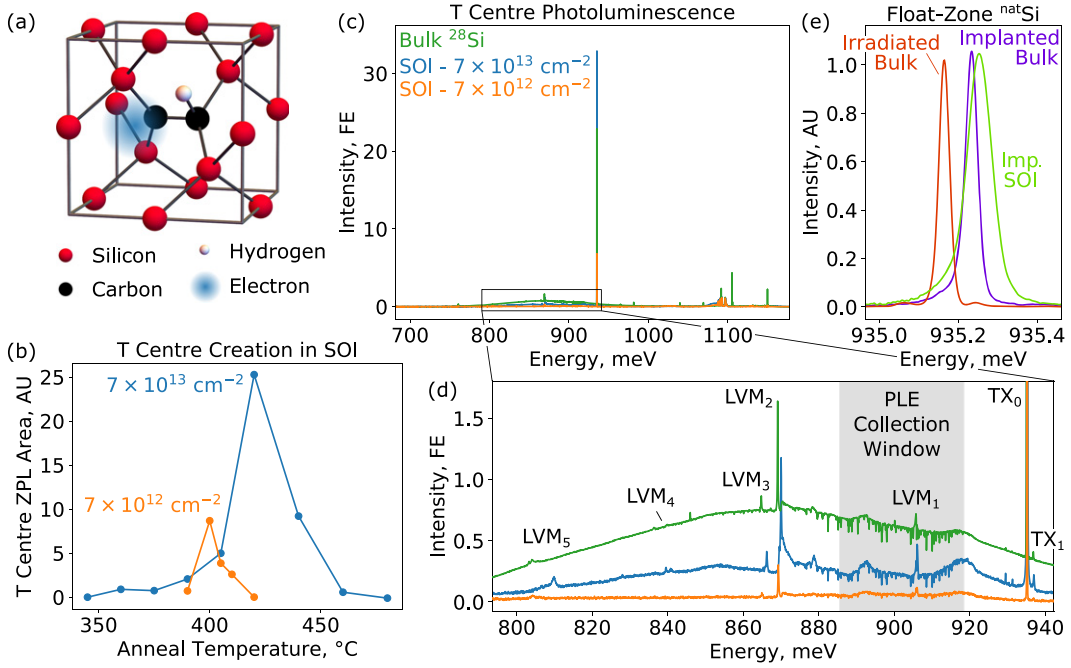

Figure 1. *T* centre implantation development. (a) Atomic structure of the *T* centre in Si as proposed in reference [24]. (b) Integrated *T* centre zero phonon line (ZPL) area in SOI as a function of the final anneal temperature. (c) and (d) *T* centre photoluminescence (PL) at a temperature of 4.2 K for bulk ^{28}Si and SOI implanted at fluences of 7×10^{12} cm^{-2} and 7×10^{13} cm^{-2}. The measured signal has been normalized to the intensity of the free exciton (FE) recombination line. Panel (d) highlights the collection window for our photoluminescence excitation (PLE) spectroscopy measurements. The sharp dips within this window are water vapour absorption lines. (e) ZPL PL for *T* centres in float-zone (FZ) ^{nat}Si (bulk and SOI) that were created either by implantation or electron irradiation. The signal has been normalized to the fitted *T* centre ZPL amplitude.

concentration of 1.5×10^{15} cm^{-3}. *T* centres were created in this bulk sample by irradiating with 320 kGy of 10 MeV electron, boiling in water for 24 h, and annealing in a hydrogen atmosphere with a 2.5 h step-wise ramp from 300°C to 440°C (additional details in the SM [7, 25]). Figure 1(d) provides a detailed view of the *T* centre sideband spectra, showing an isotopic shift in the local vibrational modes as the 7×10^{13} cm^{-2} SOI sample was implanted with ^{13}C isotopes, the 7×10^{12} cm^{-2} SOI sample was implanted with ^{12}C, and the bulk ^{28}Si sample contains a natural distribution of carbon isotopes (98.9% ^{12}C). In figure 1(d), we have also labelled both ZPLs within the *T* centre exciton doublet, where a defect-field splitting lifts TX_1 above TX_0 by 1.76 meV [7, 30].

Next, we estimate that the average *T* centre densities for the 7×10^{12} cm^{-2} and 7×10^{13} cm^{-2} SOI samples are >5 and >30 times larger than the *T* centre density in the bulk ^{28}Si sample. To compute this average density, we normalize the integrated area of the *T* centre ZPL to the nominal sample thickness. For our SOI samples, we assume a uniform *T* centre distribution and use the 220 nm device layer as our sample thickness. For our ^{28}Si sample that has *T* centres throughout its bulk, we use the 2.5 μm absorption depth of 532 nm light in silicon at cryogenic temperatures [31, 32] as the nominal sample thickness. As the FEs generated by the 532 nm excitation are not confined to the absorption region in our bulk sample, this latter thickness serves as a lower bound, making our relative concentration estimates lower bounds on the true values. We also note that this estimate of the *T* centre density neglects differences in the defects' local optical environment, such as the local index of refraction or the optical density of states, that could modify their emission properties [33]. In the SM, we verify that the implanted *T* centres are localized to the SOI device layer by selectively etching away the device layer and also by using ultraviolet PL excitation, which has a much shallower absorption depth than 532 nm light [25].

In figure 1(e), we compare the ZPL PL for *T* centres generated by implantation into bulk and SOI samples to that of *T* centres created by electron irradiation in bulk samples. All samples in this figure are FZ ^{nat}Si. Two samples were implanted with ^{13}C and hydrogen at fluences of 7×10^{12} cm^{-2}, while the third was a bulk sample that had been electron irradiated and annealed to convert native carbon and hydrogen into *T* centres [7]. We once again see the expected ^{13}C isotopic shift in the implanted ZPLs, and at 4.2 K, we report ZPL linewidths of 6.67 ± 0.09 GHz in the irradiated sample, 9.01 ± 0.08 GHz for the implanted bulk sample, and 18.0 ± 0.1 GHz for the implanted SOI sample. Moreover, the ZPL is shifted by 4.85 ± 0.03 GHz between the bulk and the SOI implanted samples. This additional broadening and shift of the ZPL in the FZ SOI likely results from additional strain in the SOI device layer [30]. As will be shown below,

the linewidths reported here lie well above the linewidth of our ^{28}Si sample and below that of our CZ SOI samples. Among these measurements, however, our bulk FZ ^{nat}Si samples provide the best comparison between implanted and irradiated linewidths as each used similar material outside both the 'semiconductor vacuum' of ^{28}Si [34] and the strained SOI device layer. We thus report that the inhomogeneous broadening for ensembles generated by ion implantation can be as little as $\sim$35% higher than for ensembles generated by electron irradiation.

3. Optical spin polarization

In other solid state emitters that lack inversion symmetry, spectral diffusion has been shown to increase when centres are generated by ion implantation [19, 35] or as centres approach interfaces due to a dramatic increase in electric and magnetic field noise in these regions [36–38]. Typically, spectral diffusion is measured by tracking spectral lines of individual emitters. Here, we develop a novel technique for measuring spectral diffusion within an ensemble of emitters and use it to compare the optical properties of the T centres in our SOI samples to those in bulk samples.

Under spin-selective resonant optical driving, the T centre ground state electron spin will polarize through a process shown schematically in figure 2(a). This unpaired electron provides a spin degree of freedom with an isotropic g-factor of $g_e = 2.005$ in the orbital ground state. Upon resonant generation of a bound exciton (BE), the ground state electron pairs with the BE electron to form a spin-0 singlet. The BE hole then provides an unpaired spin with an anisotropic g-factor g_h in the BE TX_0 state. A magnetic field B_z thus generates a spin splitting $g_e\mu_B B_z$ ($g_h\mu_B B_z$) in the ground (excited, or TX_0) state where μ_B is the Bohr magneton. Because these splittings can differ in magnitude, for Zeeman splittings $\varepsilon_B(B_z) = (\pm g_e \pm g_h)\mu_B B_z$ larger than the characteristic optical linewidth, only one spin sublevel will be excited by the resonant optical drive. Here, we define the characteristic optical linewidth to contain contributions from the excited state lifetime, thermal dephasing, and both fast and slow spectral diffusion. Spin non-conserving relaxation will then shelve the system in whichever state is not addressed by the optical drive and polarize the electron spin as the T centre is optically cycled. For the T centre, this polarization mechanism is efficient [7].

Using this process, we can reveal the characteristic optical linewidth of an ensemble by measuring how the resonantly-driven ZPL evolves in a magnetic field. In the absence of any additional broadening effects, an individual T centre's optical linewidth will approach its lifetime-limited lower bound and observable optical spin polarization at low magnetic fields is expected. This onset of optical spin polarization only weakly depends on static inhomogeneous broadening and will apply to ensembles in ^{28}Si and ^{nat}Si alike. Effects such as thermal broadening or spectral diffusion will delay this onset of optical spin polarization to larger magnetic fields as shown schematically in figure 2(b). If these mechanisms have a characteristic broadening on the same scale as the spin splitting, they will ensure that each spin sublevel is intermittently addressed by the optical field, reducing the level of spin polarization in the system and increasing the measured PL.

In figure 2(c), we perform PLE spectroscopy of the T centre ZPL in the bulk ^{28}Si sample by scanning a tunable laser over the optical resonance and measuring the PL emission within the collection window highlighted in figure 1(d). Repeating this measurement as a function of B_z, we see that, rather than Zeeman splitting along the dashed lines of figure 2(c), the PLE trace remains stationary and slowly decays as the interrogated T centre spins polarize. This measurement was performed at a temperature of 4.2 K where the ZPL linewidth is thermally-broadened [7] and with B_z aligned along the $\langle 100 \rangle$ crystal axis. For this field orientation, we expect the hole g-factors for the twelve possible T centre orientational subsets relative to $B_{\langle 100 \rangle}$ to take on the values $g_h = \{0.91, 2.55\}$ with multiplicities of 4 and 8, respectively [25, 30].

The measured spin polarization dynamics can be modelled by noting that both spin sublevels must be driven to prevent population shelving. With a magnetic field applied, the spin sublevels split by $\varepsilon_B(B_z)$ where each sublevel is assumed to have the same characteristic optical linewidth Γ. As the spin states separate and the probability of driving both sublevels decreases, the system starts to polarize. Assuming weak optical driving, we model this process with a rate model using the levels and transitions shown schematically in figure 2(d) and find that the amplitude of a partially spin-polarized PLE spectrum (figure 2(e)) is proportional to

$$A(B_z, \Delta) \propto \frac{L_B(B_z, \Delta) L_C(B_z, \Delta)}{L_B(B_z, \Delta) + L_C(B_z, \Delta)}, \tag{1}$$

where $L_{B(C)}(B_z, \Delta)$ is the Lorentzian amplitude of the spin-down (spin-up) sublevel and Δ is the optical detuning from the zero-field resonance. For simplicity, we have neglected optical transitions between states with different spin orientations, which have smaller spectral overlap with other transitions and which have

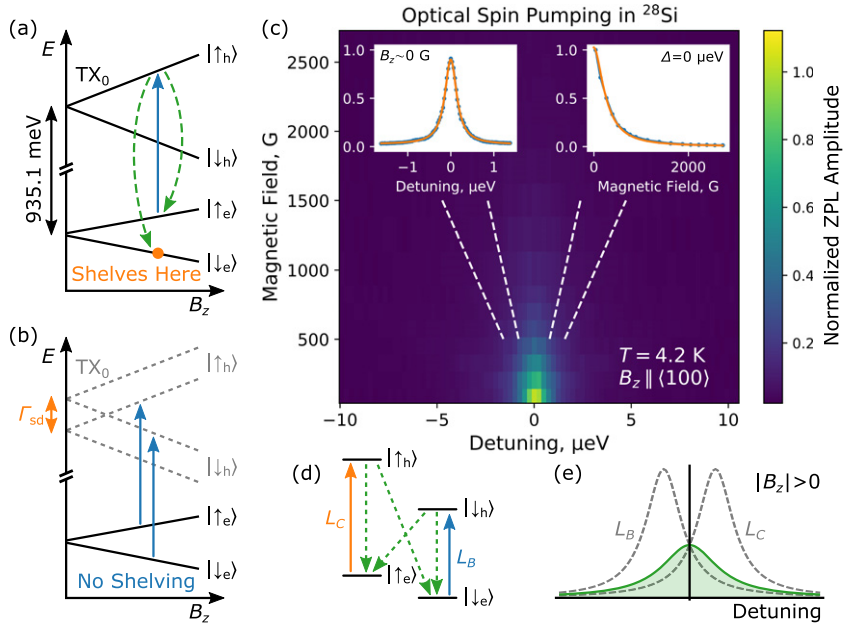

Figure 2. Optical spin polarization in T centres. (a) Optical spin polarization mechanism for T centres. (b) Depiction of how spectral diffusion can limit T centre spin polarization. (c) PLE measurements of T centres in ^{28}Si performed as a function of magnetic field at a temperature of 4.2 K. Detuning is measured from the ZPL energy of 935.062 meV. The dashed lines indicate the maximum and minimum Zeeman splittings expected for this magnetic field and sample orientation. The insets show a Lorentzian fit to the residual-field PLE spectrum and a fit of the $\Delta = 0$ μeV linecut to the spin polarization model developed in the text. (d) Levels and transitions included in the rate model for spin-dependent optical transitions. $L_{B(C)}$ represents optical excitation in the spin-down (spin-up) manifold, and the green arrows show fluorescent relaxation pathways. (e) Schematic depiction of the loss in PLE signal as a magnetic field splits the T centre spin sublevels. The resulting PL spectrum (green curve) is described by equation (1).

been shown for T centres to be much weaker than optical transitions between spin states of the same orientation [7]. The effect of these transitions is examined in the SM [25].

Evaluating equation (1) and normalizing to the $B_z = 0$, $\Delta = 0$ value, we obtain an expression for the PLE amplitude as a function of magnetic field for a single T centre:

$$A_h(B_z, \Delta) = \frac{\Gamma^2}{4\Delta^2 + \Gamma^2 + \varepsilon_B(B_z)^2}. \tag{2}$$

Because we simultaneously interrogate a large number of T centres in twelve possible orientational subsets, we model our measurement by averaging equation (2) across the twelve values of g_h. Here, we have assumed that each orientation contributes equally to the measured signal.

Fitting the data in figure 2(c) to this model, we extract a characteristic linewidth of $\Gamma = 250 \pm 100$ MHz, which agrees very well with the purely thermal linewidth of 230 MHz at 4.2 K calculated from the thermal broadening data in reference [7] as well as the $\Lambda_{\mathrm{PLE}} = 329.8 \pm 0.6$ MHz linewidth obtained by fitting the PLE spectrum in the $B_{\langle 100\rangle} = 36$ G residual magnetic field of our setup. These fits are shown in the insets to figure 2(c), and the SM provides additional plots demonstrating good agreement between the modelled and measured data [25]. The large uncertainty in Γ is dominated by uncertainties in sample alignment and in g-factor calculations as detailed in the SM [25]. Simultaneous magnetic resonance measurements in a magnetic field could address these sources of uncertainty by providing *in situ* calibration of the g-factors for an arbitrary sample orientation.

4. Spectral diffusion in bulk Si

When cooled to 1.4 K, the thermal broadening contribution to the ZPL linewidth is 33 kHz, and the ZPL PLE linewidth in the ^{28}Si sample narrows to $\Lambda_{\mathrm{PLE}} = 38 \pm 6$ MHz [25]. In the absence of significant thermal broadening, we may assume that measuring Γ amounts to measuring the total spectral diffusion linewidth Γ_{sd}. To measure Γ_{sd} at 1.4 K, we resonantly drive the T centre ZPL and ramp $B_{\langle 100\rangle}$. Fitting the normalized data shown in figure 3(a) to equation (2) averaged over the twelve orientational subsets, we find $\Gamma_{\mathrm{sd}} = 27 \pm 12$ MHz for our bulk ^{28}Si sample which agrees with the measured Λ_{PLE}. We stress the model used to analyze our ^{28}Si data only considers characteristic broadening and ignores any static inhomogeneous broadening that might be present. Moreover, our analysis ignores any inhomogeneities in Γ_{sd} that might

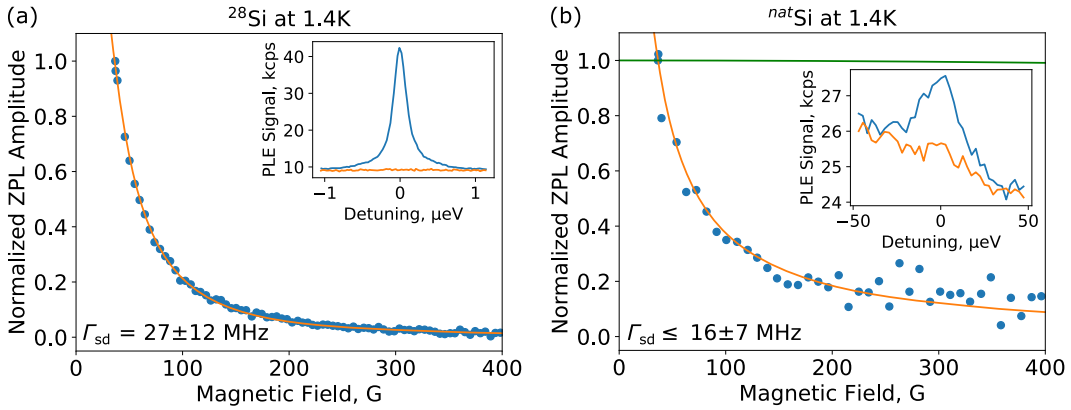

Figure 3. Spectral diffusion in bulk silicon ((a) and (b)) T centre ZPL amplitude as a function of magnetic field at a temperature of 1.4 K for (a) ^{28}Si and (b) ^{nat}Si. The data are normalized to the ZPL amplitude in the $B_{\langle 100\rangle} = 36$ G residual magnetic field of our setup. The data in (a) is fit to the model given by equation (2). The model curves in (b) assume dynamics dictated either by Γ_{sd} with static inhomogeneities (orange line) or by the PLE-measured inhomogeneous linewidth (green line). The insets in (a) and (b) show the T centre ZPL measured at $B_{\langle 100\rangle} \sim 36$ G (blue) and ∼450 G (orange). In the insets to (a) and (b), detuning is measured from the ZPL resonance at 935.064 meV and 935.167 meV, respectively.

exist amongst T centres as the effect of these inhomogeneities is expected to be small [25]. For our measurements of Γ_{sd}, we integrate PL counts for $\geqslant 1$ s at each value of $B_{\langle 100\rangle}$, making this a long-term average value of the characteristic spectral diffusion within the T centre ensemble.

To demonstrate that this method can provide a means of measuring characteristic linewidths that are not resolved in an inhomogeneously broadened PLE spectrum, we repeat this measurement on T centres in our bulk FZ ^{nat}Si sample, which has an inhomogeneously-broadened optical linewidth of $\Lambda_{PLE} = 6.0 \pm 0.2$ GHz at 1.4 K. To include this static inhomogeneous broadening in our optical spin polarization model, we replace $\Delta \rightarrow \Delta + \delta E$ in equation (2) to account for inhomogeneously-shifted resonances and convolve the result with a distribution of δE described by a Gauss–Lorentz product with a full width at half maximum equal to the measured optical linewidth Λ_{PLE}. For simplicity, we restrict ourselves to $\Delta = 0$, and once again, we model contributions from different T centre orientational subsets by averaging the calculated response over the expected distribution of g_h.

Because our single crystal ^{nat}Si sample has been cut along an unknown crystallographic axis, we can only extract an upper bound on Γ_{sd} by fitting the measured data shown in figure 3(b) as a function of magnetic field alignment and selecting the orientation that maximizes Γ_{sd} as detailed in the SM [25]. From this maximal orientation, we find $\Gamma_{sd} \leqslant 16 \pm 7$ MHz (the orange curve in figure 3(b)). For comparison, we then assume the measured decay is entirely dictated by static inhomogeneous broadening and plot the behaviour predicted by equation (2) with Γ equal to the PLE-measured inhomogeneous linewidth $\Lambda_{PLE} = 6.0$ GHz. The resulting model curve (shown in green in figure 3(b)) fails to match the data. As these models are calculated for bounding cases, we can comfortably conclude that this method extracts linewidths narrower than Λ_{PLE}.

5. Spectral diffusion in SOI

Lastly, we use this method to benchmark the optical properties of implanted T centres in CZ SOI. Increased strain in the SOI device layer compared to our bulk samples requires considering the effect of strain on these measurements. External strain can shift and mix the TX_0 and TX_1 states [30], potentially modifying g_h or generating magnetic-field dependent optical selection rules for some T centre orientational subsets. External strains principally mix states between the TX_0 and TX_1 optical branches, which are separated by a large 426 GHz defect-field splitting. Because the measured shift and inhomogeneous broadening of the T centre ZPL are both much smaller than the TX_0 and TX_1 splitting in our SOI samples, we expect the effect of strain on our measurements to be quite small [25].

At 1.4 K, the SOI samples shown in figure 1(d) display inhomogeneously-broadened ZPL linewidths of $\Lambda_{PLE} = 20.6 \pm 0.3$ GHz and 22.8 ± 0.5 GHz for the samples implanted with fluences of 7×10^{12} cm^{-2} and 7×10^{13} cm^{-2}, respectively. As shown in figure 4, we measure the PLE amplitude as a function of $B_{\langle 100\rangle}$ over the range of $B_{\langle 100\rangle}$ for which our optical setup remains stable, and we find strain-free values of $\Gamma_{sd} = 1.0 \pm 0.2$ GHz and 1.3 ± 0.3 GHz, respectively. Notably, the sample that received the lower implant fluence shows a slightly reduced level of spectral diffusion. This suggests that at least some portion of Γ_{sd} could be

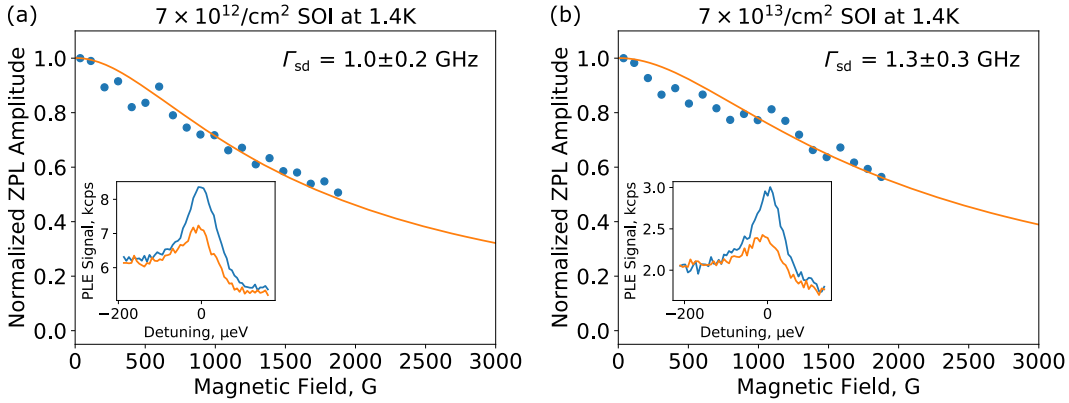

Figure 4. Spectral diffusion in SOI ((a) and (b)) T centre ZPL amplitude as a function of magnetic field at a temperature of 1.4 K for SOI implanted at a fluence of (a) 7×10^{12} cm^{-2} and (b) 7×10^{13} cm^{-2}. The data are normalized to the ZPL amplitude in the residual magnetic field of our setup. The insets show the T centre ZPL measured at $B_{\langle 100 \rangle} \sim 36$ G (blue) and ~ 2000 G (orange). In the insets to (a) and (b), detuning is measured from the ZPL resonance at 935.176 meV and 935.237 meV, respectively.

attributable to our fabrication process and might be improved with additional surface treatment [18], reduced implant fluence [35, 39], or further processing.

It is important to note that the assumption of equally weighted contributions from each T centre orientation is likely not true. For a fixed B_z direction, orientational subsets could obey different optical selection rules, creating variations in the cyclicity of the transitions amongst the orientational subsets. To address this, we have also fit our data under the assumption that the measured signal comes entirely from the T centre orientation that minimizes (maximizes) Γ_{sd} in the strain-free model to obtain the bounding sets $\Gamma_{sd} \in [0.8 \pm 0.3, 1.7 \pm 0.1]$ GHz and $\Gamma_{sd} \in [1.0 \pm 0.3, 2.1 \pm 0.1]$ GHz for the 7×10^{12} cm^{-2} and 7×10^{13} cm^{-2} samples, respectively. Once again, simultaneous magnetic resonance measurements in a magnetic field could improve the precision of this technique by calibrating the relative signal contributions of different orientations.

Even with these uncertainties, this method provides efficient comparative measurements of Γ_{sd} and rapid feedback on fabrication processes designed to reduce Γ_{sd}. Measuring PLE decay due to spin-dependent optical transitions can provide the characteristic Γ_{sd} within an ensemble of emitters when complementary techniques such as spectral hole burning [40] are not possible. Moreover, because our measurements interrogate a large ensemble of T centres simultaneously, the technique developed here enables quick access to the characteristic value of Γ_{sd} across a sample, which can be time consuming to obtain by measuring individual centres. Quick access to a sample's characteristic Γ_{sd} can enable feedback on fabrication processes to minimize Γ_{sd} and shift the distribution of single-centre Γ_{sd} to smaller values.

6. Outlook

Although far from the lifetime-limited linewidth of $\Gamma_1 = 169$ kHz [7] and $\sim$100 times larger than the values we report in bulk samples, these values for Γ_{sd} of implanted T centres in CZ SOI are already competitive with other solid state emitters near interfaces. It is common for spectral diffusion in defect centres that lack inversion symmetry to be on the order of several GHz in the absence of careful surface treatment or experimental protocols [17, 35–38]. With minimal optimization, implanted T centres display $\sim$1 GHz characteristic spectral diffusion, and this could be minimized further as fabrication and measurement techniques continue to develop. Moreover, the characteristic spectral diffusion reported here is a long-term, ensemble average. Individual centres within this ensemble could have much lower Γ_{sd} [9, 19], and any slowly varying effects that contribute to this long-term average might be addressed by feedback or filtering techniques [20, 21].

To estimate the effect spectral diffusion will have on the performance of a T centre-based photon-spin interface, we calculate the indistinguishability of two photons emitted by a given T centre as $I = \xi\Gamma_1/(\xi\Gamma_1 + \Gamma_{sd})$ where $\xi = 0.23$ is the T centre Debye–Waller factor [7, 22, 41]. For our bulk and SOI samples, respectively, we find $I \sim 2 \times 10^{-3}$ and $I \sim 4 \times 10^{-5}$. We stress that both of these values can likely be improved by employing fabrication or measurement techniques designed to stabilize the electromagnetic environment [16–19] or by filtering the emitted photons [20, 21]. Moreover, embedding T centres inside optical resonators can Purcell enhance Γ_1 to increase the photon indistinguishability. Optical resonators in

SOI capable of demonstrating Purcell factors above 10^4 have already been demonstrated [42]. Because the T centre radiative efficiency is expected to be near-unity [7], T centres incorporated into such an optical cavity could provide high quality photon-spin interfaces in the telecommunications O-band.

In summary, we have demonstrated a reliable method for using ion implantation and annealing treatments to incorporate T centres into industry-standard silicon integrated photonics material. We then developed an efficient method for using spin-dependent optical transitions to benchmark spectral diffusion. Finally, we used this new technique to show that implanted T centres within a 220 nm SOI device layer can display GHz-scale levels of spectral diffusion with minimal optimization. These results represent an important step towards developing fully-integrated quantum technologies in silicon.

Funding

This work was supported by the Natural Sciences and Engineering Research Council of Canada (NSERC), the Canada Research Chairs program (CRC), the Canada Foundation for Innovation (CFI), the BC. Knowledge Development Fund (BCKDF), the Canadian Institute for Advanced Research (CIFAR) Quantum Information Science program, the CIFAR Catalyst Fund, and Le Fonds de recherche du Québec-Nature et technologies (FRQNT). The ^{28}Si samples used in this study were prepared from the Avo28 crystal produced by the International Avogadro Coordination (IAC) Project (2004–2011) in cooperation among the BIPM, the INRIM (Italy), the IRMM (EU), the NMIA (Australia), the NMIJ (Japan), the NPL (UK), and the PTB (Germany).

Acknowledgments

We thank M L W Thewalt, L Childress, and N R Lee-Hone for fruitful discussions as well as N V Abrosimov for bulk sample growth and C Clément for rapid thermal annealing. SS is the founder and chief quantum officer of Photonic Inc. ERM, KJM and SS are employees of and participants in incentive stock plans at Photonic Inc. The other authors declare that they have no competing interests.

Data availability statement

The data that support the findings of this study are available upon reasonable request from the authors.

References

[1] Awschalom D D, Hanson R, Wrachtrup J and Zhou B B 2018 *Nat. Photonics* **12** 516
[2] Zhang G, Cheng Y, Chou J-P and Gali A 2020 *Appl. Phys. Rev.* **7** 031308
[3] Buckley S, Chiles J, McCaughan A N, Moody G, Silverman K L, Stevens M J, Mirin R P, Nam S W and Shainline J M 2017 *Appl. Phys. Lett.* **111** 141101
[4] Chartrand C, Bergeron L, Morse K J, Riemann H, Abrosimov N V, Becker P, Pohl H-J, Simmons S and Thewalt M L W 2018 *Phys. Rev.* B **98** 195201
[5] Beaufils C *et al* 2018 *Phys. Rev.* B **97** 035303
[6] Redjem W *et al* 2020 *Nat. Electron.* **3** 738
[7] Bergeron L *et al* 2020 *PRX Quantum* **1** 020301
[8] Meijer J, Burchard B, Domhan M, Wittmann C, Gaebel T, Popa I, Jelezko F and Wrachtrup J 2005 *Appl. Phys. Lett.* **87** 261909
[9] Chu Y *et al* 2014 *Nano Lett.* **14** 1982
[10] Falk A L, Buckley B B, Calusine G, Koehl W F, Dobrovitski V V, Politi A, Zorman C A, Feng P X-L and Awschalom D D 2013 *Nat. Commun.* **4** 1819
[11] Phenicie C M, Stevenson P, Welinski S, Rose B C, Asfaw A T, Cava R J, Lyon S A, de Leon N P and Thompson J D 2019 *Nano Lett.* **19** 8928
[12] Buckley S M *et al* 2020 *Opt. Express* **28** 16057
[13] Durand A *et al* 2021 *Phys. Rev. Lett.* **126** 083602
[14] Kurkjian A T K *et al* 2021 arXiv:2103.07580
[15] Muhonen J T *et al* 2014 *Nat. Nanotechnol.* **9** 986
[16] de Oliveira F F, Antonov D, Wang Y, Neumann P, Momenzadeh S A, Häußermann T, Pasquarelli A, Denisenko A and Wrachtrup J 2017 *Nat. Commun.* **8** 15409
[17] Anderson C P *et al* 2019 *Science* **366** 1225
[18] Sangtawesin S *et al* 2019 *Phys. Rev.* X **9** 031052
[19] Kasperczyk M *et al* 2020 *Phys. Rev.* B **102** 075312
[20] Bernien H *et al* 2013 *Nature* **497** 86
[21] Guo K, Springbett H, Zhu T, Oliver R A, Arakawa Y and Holmes M J 2019 *Appl. Phys. Lett.* **114** 112109
[22] Grange T, Hornecker G, Hunger D, Poizat J-P, Gérard J-M, Senellart P and Auffèves A 2015 *Phys. Rev. Lett.* **114** 193601
[23] Giesz V *et al* 2015 *Phys. Rev.* B **92** 161302
[24] Safonov A N, Lightowlers E C, Davies G, Leary P, Jones R and Öberg S 1996 *Phys. Rev. Lett.* **77** 4812

[25] See Supplementary Information.
[26] Pichler P 2004 Isovalent impurities *Intrinsic Point Defects, Impurities, and Their Diffusion in Silicon* (Berlin: Springer) pp 281–329
[27] Berhanuddin D D, Lourenço M A, Gwilliam R M and Homewood K P 2012 *Adv. Funct. Mater.* **22** 2709
[28] Ohmura Y, Takahashi K, Saitoh H, Kon T and Enosawa A 1999 *Physica* B **273–274** 228
[29] Colley P M and Lightowlers E C 1987 *Semicond. Sci. Technol.* **2** 157–66
[30] Safonov A N, Lightowlers E C and Davies G 1995 *Mater. Sci. Forum* **196–201** 909
[31] Dash W C and Newman R 1955 *Phys. Rev.* **99** 1151
[32] Jellison G E Jr and Joshi P C 2018 *Spectroscopic Ellipsometry for Photovoltaics* (Berlin: Springer) ch 8
[33] Barnes W L 1998 *J. Mod. Opt.* **45** 661
[34] Saeedi K *et al* 2013 *Science* **342** 830
[35] van Dam S B *et al* 2019 *Phys. Rev.* B **99** 161203
[36] Ishikawa T, Fu K-M C, Santori C, Acosta V M, Beausoleil R G, Watanabe H, Shikata S and Itoh K M 2012 *Nano Lett.* **12** 2083
[37] Evans R E, Sipahigil A, Sukachev D D, Zibrov A S and Lukin M D 2016 *Phys. Rev. Appl.* **5** 044010
[38] Crook A L *et al* 2020 *Nano Lett.* **20** 3427
[39] Wolfowicz G, Heremans F J, Anderson C P, Kanai S, Seo H, Gali A, Galli G and Awschalom D D 2020 arXiv:2010.16395
[40] Völker S 1989 *Annu. Rev. Phys. Chem.* **40** 499
[41] Bylander J, Robert-Philip I and Abram I 2003 *Eur. Phys. J.* D **22** 295
[42] Md Zain A R, Johnson N P, Sorel M and De La Rue R M 2008 *Opt. Express* **16** 12084